electronics

MDPI

Article

Initial Development and Analysis of a Context-Aware Burn Resuscitation Decision-Support Algorithm

Yi-Ming Kao [1], Ghazal Arabidarrehdor [1], Babita Parajuli [2], Eriks E. Ziedins [3], Melissa M. McLawhorn [3], Cameron S. D'Orio [3], Mary Oliver [3], Lauren Moffatt [3,4], Shane K. Mathew [3], Edward J. Kelly [3], Bonnie C. Carney [3,4], Jeffrey W. Shupp [3,4,5], David M. Burmeister [2] and Jin-Oh Hahn [1,*]

[1] Department of Mechanical Engineering, University of Maryland, College Park, MD 20742, USA; ymkao@umd.edu (Y.-M.K.); ghazal.abdd.aut@gmail.com (G.A.)
[2] Department of Medicine, Uniformed Services University of the Health Sciences, Bethesda, MD 20814, USA; babita.parajuli.ctr@usuhs.edu (B.P.); david.burmeister@usuhs.edu (D.M.B.)
[3] Firefighters' Burn and Surgical Research Laboratory, MedStar Health Research Institute, Washington, DC 20010, USA; eriks.e.ziedins@medstar.net (E.E.Z.); melissa.m.mclawhorn@medstar.net (M.M.M.); cameron.s.dorio@medstar.net (C.S.D.); mary.oliver@vanderbilt.edu (M.O.); lauren.t.moffatt@medstar.net (L.M.); shanekmathew@gmail.com (S.K.M.); edward.kelly1@email.gwu.edu (E.J.K.); bonnie.c.carney@medstar.net (B.C.C.); jeffrey.w.shupp@medstar.net (J.W.S.)
[4] Departments of Surgery and Biochemistry, Georgetown University School of Medicine, Washington, DC 20007, USA
[5] The Burn Center, Department of Surgery, MedStar Washington Hospital Center, Washington, DC 20010, USA
* Correspondence: jhahn12@umd.edu

Abstract: Burn patients require high-volume intravenous resuscitation with the goal of restoring global tissue perfusion to make up for burn-induced loss of fluid from the vasculature. Clinical standards of burn resuscitation are predominantly based on urinary output, which is not context-aware because it is not a trustworthy indicator of tissue perfusion. This paper investigates the initial development and analysis of a context-aware decision-support algorithm for burn resuscitation. In this context, we hypothesized that the use of a more context-aware surrogate of tissue perfusion may enhance the efficacy of burn resuscitation in normalizing cardiac output. Toward this goal, we exploited the arterial pulse wave analysis to discover novel surrogates of cardiac output. Then, we developed the cardiac output-enabled burn resuscitation decision-support (CaRD) algorithm. Using experimental data collected from animals undergoing burn injury and resuscitation, we conducted an initial evaluation and analysis of the CaRD algorithm in comparison with the commercially available Burn Navigator™ algorithm. Combining a surrogate of cardiac output with urinary output in the CaRD algorithm has the potential to improve the efficacy of burn resuscitation. However, the improvement achieved in this work was only marginal, which is likely due to the suboptimal tuning of the CaRD algorithm with the limited available dataset. In this way, the results showed both promise and challenges that are crucial to future algorithm development.

Keywords: decision support; burn injury; resuscitation; neural network; cardiac output; pulse pressure variation

check for updates

Citation: Kao, Y.-M.; Arabidarrehdor, G.; Parajuli, B.; Ziedins, E.E.; McLawhorn, M.M.; D'Orio, C.S.; Oliver, M.; Moffatt, L.; Mathew, S.K.; Kelly, E.J.; et al. Initial Development and Analysis of a Context-Aware Burn Resuscitation Decision-Support Algorithm. *Electronics* **2024**, *13*, 2713. https://doi.org/10.3390/electronics13142713

Academic Editor: William M. Mongan

Received: 17 May 2024
Revised: 21 June 2024
Accepted: 2 July 2024
Published: 11 July 2024

Copyright: © 2024 by the authors. Licensee MDPI, Basel, Switzerland. This article is an open access article distributed under the terms and conditions of the Creative Commons Attribution (CC BY) license (https://creativecommons.org/licenses/by/4.0/).

1. Introduction

Burn injury is associated with a complex array of inflammation and endothelial dysfunction, which result in a massive shift of plasma from the intravascular space to the tissues [1–3]. Burn patients are resuscitated with the infusion of intravenous (IV) fluid (mostly with Lactated Ringer's (LR)) [4,5]. However, a non-significant portion of the IV fluid is also shifted to the tissues due to vascular leakage and other pathophysiology [6]. Recommendations intended to standardize burn resuscitation exist [7,8]. However, treatment given to each patient must be personalized due to large inter-individual variability

in pre-existing conditions and physiological responses to burn injury [9]. In many burn centers, burn resuscitation starts with standardized IV fluid rates, which are then titrated to maintain urinary output (UO) within a desired range. [10,11]. However, the existing literature indicates that UO is not an ideal surrogate of blood volume (BV) and cardiac output (CO) [12–15]. Since burn resuscitation aims at restoring BV and CO (which are reduced due to capillary leak), burn resuscitation must ideally be titrated to direct surrogates of BV and CO.

Arterial pulse waveform analysis (PWA) has been extensively investigated in the context of hemorrhage as a means to infer fluid responsiveness, including the pulse pressure variation (PPV) [16–18], the Compensatory Reserve Index (CRI) [19–21], the BV decompensation status (BVDS) index [22,23], and various arterial PWA features [24–27] to list a few. However, none of these innovative metrics had been rigorously evaluated in the context of burn resuscitation until recently. Specifically, it remains unknown if these metrics are (i) useful for guiding burn resuscitation treatment, (ii) superior to UO, and (iii) complementary to UO in understanding BV and CO status in burn injury patients.

In our recent work, we demonstrated that PPV, systolic pressure variation (SPV), and certain PWA features may complement UO in inferring the adequacy of burn resuscitation status in large animals [28]. In addition, PPV measurement is commercially available. The promise and accessibility of PPV motivated us to hypothesize that it may be possible to incorporate PPV (and, in the longer term, arterial PWA features) into burn resuscitation to enable superior personalized and more context-aware titration of IV fluid rates. To test this hypothesis, we developed and conducted an initial evaluation and analysis of a CO-enabled burn resuscitation decision-support (CaRD) algorithm, which is a data-driven algorithm exploiting PPV and UO to infer CO and then titrate burn resuscitation based on the CO estimate. We developed the CaRD algorithm using experimental data collected from 21 pigs. Then, we conducted a prospective initial evaluation and analysis of the CaRD algorithm in comparison with the commercially available Burn Navigator^{TM} (BN) algorithm in nine pigs. To the best of our knowledge, the use of context-aware PWA features in the context of burn resuscitation has not been explored in the existing literature. Hence, the novelty of our current work lies in the first exploitation of a context-aware surrogate of tissue perfusion in the development of a data-driven burn resuscitation decision-support algorithm superior to the state-of-the-art one based on UO alone.

This paper is organized as follows. Section 2 details the development, evaluation, and analysis of the CaRD algorithm. Section 3 presents key results, and its discussion. Section 4 concludes the paper with future directions.

2. Methods

2.1. Development Dataset

To develop the CaRD algorithm, we used the dataset collected in our prior work [28]. The dataset is composed of experimental data collected from 21 female pigs (weight: 32 ± 4 kg). After regulatory approval, the animals were anesthetized and then subjected to 40% total burn surface area (TBSA) burn and assigned randomly to one of the following three resuscitation protocols: (i) no resuscitation; (ii) resuscitation given based on the recommendation by the BN algorithm using IV LR to maintain UO within a goal range of 1.0–1.5 mL/h/kg to adequately treat the animal; and (iii) resuscitation given using IV LR at $\geq$500 mL/h to over-resuscitate the animal. All the animals remained anesthetized and were monitored continuously for 24 h post-burn. Measurements included hourly UO, central venous blood pressure (BP) (CVP) and IV fluid infusion rate, continuous arterial BP waveforms, and CO at 0, 3, 6, 9, 12, 15, 18, 21, and 24 h post-burn. Note that at some hours in some animals, CO could not be obtained due to the loss of Swan–Ganz catheter access during the experiments. We used all the CO measurements in the development of the CaRD algorithm. Full details of the experimental protocol, including anesthesia, instrumentation, and injury and resuscitation procedures, can be found in our prior work [28].

We preprocessed the dataset and calculated PWA features, including PPV, as described in our prior work [28]. Then, we used these experimental data to develop the CaRD algorithm. A unique strength of this dataset is its inclusion of diverse resuscitation protocols, which makes it possible to encompass a wide range of resuscitation regimes (namely, extreme dehydration to extreme over-hydration) in the development of the CaRD algorithm.

2.2. Cardiac Output-Enabled Burn Resuscitation Decision-Support Algorithm

Figure 1 shows the schematic of the CaRD algorithm. At each hour, the CaRD algorithm receives hourly average PPV and UO and then performs the following operations. First, it normalizes PPV and UO. Second, it infers weight-normalized CO based on the normalized PPV and UO. Third, it computes the IV fluid infusion rate recommended during the next hour based on a variant of the commercially available BN algorithm. In this regard, our hypothesis was that burn resuscitation may be better guided by CO than UO. This hypothesis is plausible in that (i) CO is a direct surrogate of tissue perfusion, whereas (ii) UO is a controversial surrogate of tissue perfusion despite its widespread use in current burn resuscitation. This section describes the details of these operations.

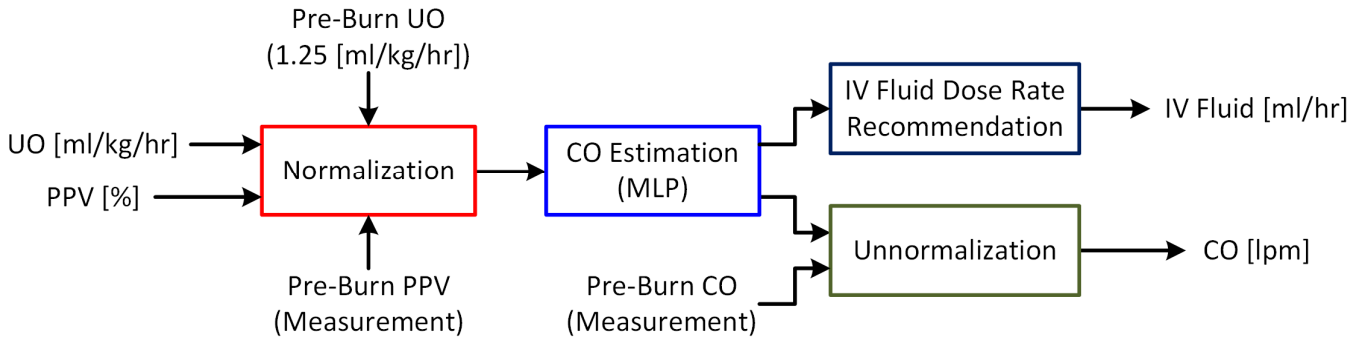

Figure 1. Cardiac output-based burn resuscitation decision-support (CaRD) algorithm. MLP: multilayer perceptron.

2.2.1. Normalization

The CaRD algorithm is built upon weight-normalized UO and CO to cancel the weight-dependent variability. In addition, the weight-normalized UO and CO, as well as PPV, are normalized further so that their values are close to zero if resuscitated adequately, positive if over-resuscitated, and negative if under-resuscitated. A patient is defined as adequately resuscitated if CO is restored to its pre-burn level. The CaRD algorithm normalizes the weight-normalized UO inputted to it as follows:

$$\tilde{U} = \frac{U - U_0}{\sigma_U}, \tag{1}$$

where U is weight-normalized UO, $\tilde{U}$ is normalized UO, and U_0 and σ_U are the intercept and spread factors determined based on the range of target UO widely used in the context of burn resuscitation as pre-burn normal level (1.0–1.5 mL/kg·h) [29,30]. The CaRD algorithm normalizes PPV input to it on a patient-by-patient basis based on (i) the pre-burn measurement pertaining to each patient as intercept and (ii) the standard error of the pre-burn measurements pertaining to a cohort of patients (which, in our work, is the standard error of pre-burn PPV in all the animals in the development dataset) as spread factor:

$$\tilde{\delta P_p} = -\frac{\delta P_p - \delta P_{p0}}{\sigma_{\delta P_p}}, \tag{2}$$

where δP_p is PPV, $\widetilde{\delta P_p}$ is normalized PPV, δP_{p0} is patient-specific pre-burn PPV, and $\sigma_{\delta P_p}$ is the standard error of PPV. Using these normalized UO and PPV, the CaRD algorithm estimates CO normalized in the same way:

$$\widetilde{Q} = \frac{Q - Q_0}{\sigma_Q}, \tag{3}$$

where Q is weight-normalized CO, $\widetilde{Q}$ is normalized CO, Q_0 is patient-specific pre-burn CO, and σ_Q is the standard error of CO. Section 2.2.2 describes how the CaRD algorithm estimates CO in Equation (3) using UO in Equation (1) and PPV in Equation (2).

2.2.2. Cardiac Output Estimation

The CaRD algorithm infers weight-normalized CO by exploiting PPV and UO normalized in Equations (1) and (2). The exact mechanistic relationship between PPV, UO, and CO is unknown, which makes the use of a model-based approach highly challenging. Hence, we pursued a data-driven approach in which we developed a multi-layer perceptron (MLP) that regresses PPV and UO to CO. The development dataset included only 144 input–output data pairs ({PPV, UO, CO}) available to train the MLP (seven data pairs per animal on average). Hence, we restricted the complexity of the MLP and introduced synthetic input–output data pairs to prevent overfitting as follows. First, we considered a single hidden layer. In addition, we limited the number of neurons in the hidden layer to $\leq$9, given that nine neurons in the hidden layer result in 37 trainable parameters in the MLP. Second, we introduced synthetic input–output data pairs to facilitate adequate MLP regression around the origin (i.e., to make MLP pass through the origin). Our inspection of the input–output data pair revealed that we lacked input–output data pairs in the vicinity of the origin (i.e., $\left\{\widetilde{U}, \widetilde{\delta P_p}, \widetilde{Q}\right\} = \{0, 0, 0\}$) due to the small number of input–output data pairs covering a wide range of resuscitation regimes. Such a lack of input–output data pairs around the origin made the regression task challenging, especially by entailing bias in the MLP around the origin. Indeed, the MLP regression to the 144 input–output data pairs alone resulted in MLP whose output non-trivially deviated from zero even when $\widetilde{U} = \widetilde{\delta P_p} = 0$. Based on the inspection of the coverage provided by the 144 available input–output data pairs, we introduced a pre-specified number of synthetic input–output data pairs $\left\{\widetilde{U}, \widetilde{\delta P_p}, \widetilde{Q}\right\} = \left\{\left(\epsilon_U, \epsilon_{P_p}, \epsilon_Q\right)\right\}$, where $\epsilon_U \sim \mathcal{N}(0, 2.5)$, $\epsilon_{P_p} \sim \mathcal{N}(0, 2.5)$, and $\epsilon_Q = \frac{\epsilon_U + \epsilon_{P_p}}{\varepsilon_Q}$, where ε_Q is a tunable hyper-parameter. The number of synthetic input–output data pairs must be carefully chosen to help MLP pass through the origin while minimizing the undesired distortion of the input–output relationship regressed by MLP.

We regarded the number of neurons in the hidden layer, the number of synthetic input–output data pairs, and ε_Q as hyper-parameters in the CaRD algorithm. We tuned these hyper-parameters in the course of developing an optimal MLP using the development dataset as described in Section 2.2.4 in order to achieve two goals. First, the MLP must properly regress the input–output relationship between UO and PPV vs. CO. Second, the resulting CaRD algorithm must recommend IV fluid infusion rates in the correct direction (e.g., the rate is increased when CO is below pre-burn level while the rate is decreased when CO is above pre-burn level) by an appropriate amount (i.e., comparable to the BN algorithm).

2.2.3. Dose Recommendation

To develop the IV fluid dose recommendation element in the CaRD algorithm, we leveraged the so-called BN algorithm [31,32]. The BN algorithm provides a patented and commercially available dose recommendation formula solely based on UO applicable to

the resuscitation of burn patients. The original dose recommendation formula pertaining to the BN algorithm is given by the following:

$$\begin{aligned} I(t) &= I(t-1) + e(t) \times \left(-\frac{k_I(t)}{k_{UO}}\right) \times Y_W \times Y_{TBSA} \times G_{UO}, \\ Y_W &= 0.001 + \frac{1.2}{\left[1+7e^{-0.2(W-93)}\right]^7}, \\ Y_{TBSA} &= 0.001 + \frac{1.2}{\left[1+2e^{-0.2(TBSA-33)}\right]^2}, \\ G_{UO} &= 1 - e^{-\left[\frac{e(t)}{5}\right]^2}, \end{aligned} \tag{4}$$

where $I(t)$ is the recommended IV fluid infusion rate at a time instant t (in hours post-burn); $e(t) = U(t) - U_D$ is the error between the UO at a time instant t and the desired UO (40 mL); $k_I(t)$ is the infusion rate constant at a time instant t (which is -36.53 if $0 \leq t \leq 13$ and -21.55 if $14 \leq t \leq 33$); k_{UO} is the UO constant (which is set to 1.211); Y_W is the weight modifier to account for the effect of weight W; Y_{TBSA} is the TBSA modifier to account for the effect of TBSA; and G_{UO} is a Gaussian function centered at the desired UO. To realize the dose recommendation element in the CaRD algorithm, we replaced UO in Equation (4) with the normalized CO outputted by the MLP in Section 2.2.2. Hence, the dose recommendation formula pertaining to the CaRD algorithm is given by the following:

$$\begin{aligned} I(t) &= I(t-1) + \alpha \times \widetilde{Q}(t) \times \left(-\frac{k_I(t)}{k_{UO}}\right) \times Y_W \times Y_{TBSA} \times G_{CO}, \\ Y_{weight} &= 0.001 + \frac{1.2}{\left(1+7e^{-0.2(X_{weight}-93)}\right)^7}, \\ Y_{tbsa} &= 0.001 + \frac{1.2}{\left(1+2e^{-0.2(X_{tbsa}-33)}\right)^2}, \\ G_{CO} &= 1 - e^{-\left[\frac{\widetilde{Q}(t)}{5}\right]^2}, \end{aligned} \tag{5}$$

where $\widetilde{Q}(t)$ is the estimated normalized CO at a time instant t; α is the CaRD gain representing the sensitivity of the dose recommendation formula to its input; and G_{CO} is the Gaussian function centered at the desired normalized CO (namely, zero).

We regarded the CaRD gain α as a hyper-parameter in the CaRD algorithm. We tuned the CaRD gain using the development dataset so that the resulting CaRD algorithm can recommend IV fluid infusion rates in the correct direction (e.g., the rate is increased when CO is below pre-burn level while the rate is decreased when CO is above pre-burn level) by an appropriate amount (i.e., comparable to the BN algorithm) (see Section 2.2.4).

2.2.4. Algorithm Tuning

As mentioned above, the CaRD algorithm includes four hyper-parameters to be tuned, namely the number of neurons in the hidden layer, the number of synthetic input–output data pairs, ε_Q, and the CaRD gain α. We tuned these hyper-parameters as follows to develop the CaRD algorithm that is ready for prospective evaluation and analysis. First, we specified the ranges associated with all the hyper-parameters to be explored in optimizing the CaRD algorithm: (i) the number of neurons in the hidden layer m_N ranged between 1 and 9 to restrict the number of trainable parameters in the MLP to $\leq$37 (see Section 2.2); (ii) the number of synthetic input–output data pairs m_D between 10 and 50 by trial and error to prevent their adverse impact on the MLP regression (namely, its excessive distortion around the origin); (iii) ε_Q between 1 and 10 by trial and error to likewise prevent their adverse impact on the MLP regression (namely, its excessive distortion around the origin); and (iv) α between 10 and 100 to make $e(t) \times G_{UO}$ in Equation (4) and $\alpha \times \widetilde{Q}(t) \times G_{CO}$ in Equation (5) comparable in magnitude. Second, while sweeping the hyper-parameters in these ranges, we repeatedly implemented the CaRD algorithm, as shown in Figure 1, by combining the normalization (Section 2.2.1), the MLP for CO estimation (Section 2.2.2) with m_N neurons in its hidden layer, and the dose recommen-

dation formula in Equation (5) (Section 2.2.3) with the CaRD gain α. Third, we trained the MLP by maximizing the goodness of fit between measured weight-normalized CO ($\widetilde{Q}$ in Equation (3)), as well as m_D synthetic weight-normalized CO generated with ε_Q vs. the corresponding weight-normalized CO predicted by the MLP based on weight-normalized UO ($\widetilde{U}$ in Equation (1)) and PPV ($\widetilde{\delta P_p}$ in Equation (2)). We used MATLAB 2020b and its Neural Network Toolbox for this task. Fourth, we input all the 144 UO–PPV pairs in the development dataset to the CaRD algorithm equipped with the trained MLP, and the CaRD gain α and calculated the change in the hourly IV fluid infusion rate, i.e., $\Delta I(t) = I(t) - I(t-1) = \alpha \times \widetilde{Q}(t) \times \left(-\frac{k_I(t)}{k_{UO}}\right) \times Y_W \times Y_{TBSA} \times G_{CO}$. Fifth, we calculated the two performance metrics below using the resulting 144 $\Delta I(t)$ values:

(1) Explainability: The explainability metric is defined as the percentage of the 144 $\Delta I(t)$ values that are explainable. A $\Delta I(t)$ value is explainable if (i) $\Delta I(t) \geq 0$ when $\widetilde{Q} \leq 0$ or (i) $\Delta I(t) < 0$ when $\widetilde{Q} > 0$. Ideally, the explainability metric must be 100%.

(2) Aggressiveness: The aggressiveness metric is defined as the degree of change in the hourly IV fluid infusion rate, measured in terms of average $|\Delta I(t)|$ values. Considering that our no-resuscitation protocol intentionally uses $I(t) = 0$ (and accordingly, $\Delta I(t) = 0$), while our over-resuscitation protocol intentionally uses overly and consistently aggressive $I(t)$, we measured the aggressiveness metric using a subset of the development dataset pertaining to BN-based resuscitation (52 $\Delta I(t)$ values). Ideally, the aggressiveness metric must not be too large or too small in comparison with the aggressiveness metric pertaining to the BN algorithm (which is not the best algorithm but is still an adequate algorithm).

Sixth, we selected the best-performing CaRD algorithm to be employed for preliminary evaluation and analysis as the one associated with a large explainability metric, an aggressiveness metric similar to that of the BN algorithm (which can be readily calculated using Equation (4)), and a smooth MLP regression map relating UO and PPV to CO (which may imply a low likelihood of overfitting). We assessed the smoothness of the MLP by visual inspection of the 3-D regression map.

2.3. Prospective Algorithm Evaluation and Analysis

We prospectively evaluated the performance of the CaRD algorithm and compared it with the BN algorithm by conducting experiments in nine female pigs (weight: 32 ± 2 kg). This research was approved by the MedStar Health Research Institutional Animal Care and Use Committee (IACUC) and performed at an AAALAC fully accredited facility. All animal procedures were conducted in compliance with the Guide for the Care and Use of Laboratory Animals and the Animal Welfare Act. The experimental protocol, including anesthesia, instrumentation, and injury and resuscitation procedures, was consistent with our prior work [28]. In brief, all the animals were anesthetized and then subjected to 40% TBSA burn and assigned randomly to the CaRD algorithm group (five pigs) or the BN algorithm group (four pigs). In the CaRD algorithm group, at each hour after inducing the burn up to 24 h, we measured hourly average UO and PPV (B1X5M Patient Monitor Systems with VSP 3.0 Software Upgrade, GE Healthcare), estimated CO, calculated the recommended IV fluid infusion rate, and manually changed the IV fluid infusion rate accordingly. In the BN algorithm group, at each hour after inducing the burn up to 24 h, we likewise measured hourly average UO, calculated the recommended IV fluid infusion rate, and manually changed the IV fluid infusion rate accordingly. To minimize potentially detrimental and confounding physiological effects, we limited the change in the hourly IV fluid infusion rate (i.e., $\Delta I(t)$) to ±20% (Animals 2–6, 2–7, and 2–10) or ±10% (Animals 2–12 and 2–13) of the IV fluid infusion rate during the previous hour (i.e., $I(t-1)$). In both groups, we measured hourly UO, CVP, and IV fluid infusion rate, continuous arterial BP waveform, and CO at 0, 3, 6, 9, 12, 15, 18, 21, and 24 h post-burn. Note that at some hours in some animals, CO could not be obtained due to the loss of Swan–Ganz catheter access during the experiments. We used all the CO measurements in the development of

the CaRD algorithm. The number of CO measurements was 36 in the CaRD algorithm group and 34 in the BN algorithm group.

Using the experimental results, we evaluated the performance of the CaRD algorithm by calculating two metrics. First, we calculated the normalized mean absolute error (NMAE) of 24, 12, and 9 h post-burn CO measurements with respect to the animal's pre-burn CO measurement in each animal. Second, we calculated the in-range CO rate in each animal, defined as the number of post-burn CO measurements within the range of interest (given by $|\widetilde{Q}| \leq \widetilde{Q}_{threshold}$, where $\widetilde{Q}_{threshold}$ is the threshold specifying the in-range) divided by the total number of post-burn CO measurements. Then, we calculated the statistics of these measures across all the animals. Note that both metrics indicate the efficacy of the CaRD algorithm in restoring CO post-burn back to its pre-burn level. For the sake of comparison, we calculated the statistics of the NMAE of 24, 12, and 9 h post-burn CO measurements with respect to the animal's pre-burn CO measurement pertaining to the BN algorithm. We compared the descriptive statistics pertaining to these two metrics between the CaRD algorithm vs. the BN algorithm. However, we did not perform statistical tests due to the small sample size.

Using the experimental results, we also conducted an initial analysis of the CaRD algorithm in order to understand its behavior. Our analysis encompassed individual elements in the CaRD algorithm, including (i) input normalization, (ii) CO estimation, and (iii) IV fluid dose recommendation. First, we compared the spread factors pertaining to PPV and CO in Equations (2) and (3) derived using the development dataset with the standard errors of PPV and CO derived from the nine test animals. The reason for this analysis is the potential influence of the spread factors on the gain of the CaRD algorithm. For example, the CaRD algorithm trained with the development dataset may be overly sensitive to PPV and, consequently, recommend overly aggressive resuscitation if the spread factors derived using the development dataset are substantially small relative to those derived from the nine test animals. Second, we quantified the accuracy of the MLP for CO estimation. The reason for this analysis is the potential influence of the CO estimation accuracy on the overall performance of the CaRD algorithm. For example, the CaRD algorithm may perform better resuscitation as CO estimation accuracy gets better. As an ancillary analysis, we developed and evaluated an MLP based on the most powerful PWA feature found in our prior work [28] (namely, $\frac{P_m - P_d}{T}$, where P_m and P_d are mean and diastolic BP and T is heart period), in order to examine if CO can be inferred well from the combination of a PWA feature and UO (including PPV and UO). Third, we compared the gain associated with dose recommendation pertaining to the CaRD algorithm and the BN algorithm. Specifically, we comparatively examined the distributions (in terms of histograms) of normalized CO (CaRD) and normalized UO (BN), as well as those of the recommended changes in hourly IV fluid infusion rates. The reason for this analysis is the potential influence of the gain of dose recommendation on the overall aggressiveness of CaRD and BN algorithms. Finally, we consolidated the results from all these analyses to identify which aspect(s) in the CaRD algorithm must be improved to make it more efficacious.

3. Results and Discussion

The ultimate goal of burn resuscitation is to mitigate burn shock by restoring blood perfusion to end organs. This is done by compensating for the intravascular fluid loss resulting from the burn-induced inflammatory storm and endothelialopathy [33]. Existing burn resuscitation protocols are built upon UO, which is not an effective surrogate of tissue perfusion and is thus not context-aware. In our attempt to address this challenge, we developed and conducted an initial evaluation and analysis of the CaRD algorithm, in which the IV fluid rate is recommended based on CO estimated from PPV and UO. In this context, the main novelty of our current work lies in the exploitation of a context-aware surrogate of tissue perfusion (namely, PPV) in conjunction with conventional UO in the development of a data-driven burn resuscitation decision-support algorithm based on CO estimation. Details follow.

3.1. Algorithm Development

We used data collected from pigs as development dataset. While the typical renal clearance in pigs is slightly higher than in humans [34], pigs offer several advantages than, for example, rodents due to the cutaneous structure and arterial capacity (i.e., ability to use clinically relevant catheters) and are thus used more often for burn resuscitation [35].

Due to the limited amount of development dataset, we used the development dataset in its entirety to derive and optimize the CaRD algorithm (including the tuning of its hyper-parameters). We used 1.25 mL/kg·h as U_0 and 0.25 mL/kg·h as σ_U in Equation (1) based on the publicly known UO range used as a target for burn resuscitation (1.0–1.5 mL/kg·h) [29,30]. We observed a large inter-individual variability in PPV and CO across the animals in the development dataset. Hence, we used animal-specific pre-burn PPV and CO values as δP_{p0} in Equation (2) and Q_0 in Equation (3), while we used the standard errors pertaining to the pre-burn δP_{p0} (1.3%) and Q_0 (9.0 mL/min/kg) values across all the animals as $\sigma_{\delta P_p}$ in Equation (2) and σ_Q in Equation (3). During the development stage, whether the chosen $\sigma_{\delta P_p}$ and σ_Q values were reasonable was not known in the absence of any preliminary data. Hence, we assessed the adequacy of these values using the results obtained from the prospective algorithm evaluation (see Section 3.3).

Armed with the tuned hyper-parameter values ($m_N = 7$, $m_D = 20$, $\varepsilon_Q = 4$, and $\alpha = 40$), the CaRD algorithm exhibited an adequate performance (Figure 2 and Table 1). Table 1 shows the explainability and aggressiveness metrics associated with the CaRD algorithm and the BN algorithm (see Section 2.2.4). The CaRD algorithm showed higher explainability than the BN algorithm, meaning that the former provided explainable IV fluid infusion rate recommendations more frequently than the latter (Table 1). In addition, the CaRD algorithm showed qualitatively comparable aggressiveness to the BN algorithm, meaning that at least it may not recommend the changes in IV fluid infusion rate, which are too extreme (Table 1). The CO estimation accuracy was perhaps adequate but not superb (RMSE: 2.89 [·]; r value: 0.62 [·]; see Figure 2 with $m_N = 7$). Figure 2 shows the dependence of the goodness of fit of the MLP (in terms of root-mean-squared error (RMSE) and correlation coefficient between measured vs. estimated CO) on the number of neurons in its hidden layer. As can be seen, 7–9 neurons (amounting to 29–37 trainable parameters in the MLP) appear to be associated with a local optimum. According to Figure 2, CO estimation accuracy may be improved with a further increase in the number of neurons in the hidden layer. However, we observed an increasing degree of crumpling of the regression map, which is indicative of over-fitting.

Figure 3 shows the regressed MLP mapping between normalized UO, normalized PPV, and normalized CO. As can be seen, estimated normalized CO is monotonically proportional to both normalized UO and normalized PPV in general (note that PPV is known to decrease as a patient gets over-resuscitated [36] and that normalized PPV and PPV are inversely proportional due to the negative sign in Equation (2); hence, a large normalized PPV plausibly implies a large normalized/unnormalized CO). However, the mapping also exhibits modest biphasic behavior with respect to normalized PPV. For example, when normalized UO is zero, normalized CO increases as normalized PPV increases from -5 up to approximately 4. Then, when the normalized PPV is between 4 and 9, normalized CO decreases and again increases back to its level when the normalized PPV is 4. Finally, when normalized PPV is greater than 9, normalized CO is again proportional to normalized PPV. This undesirable behavior may be attributed to the unexplainable input–output data pairs (see Table 2). The biphasic behavior appears to have been suppressed in the region where the synthetic input–output data pairs were used ($-2.5 \leq \widetilde{U} \leq 2.5$ and $-2.5 \leq \widetilde{\delta P_p} \leq 2.5$), which suggests the adequacy of these synthetic input–output data pairs in deriving an explainable regression mapping.

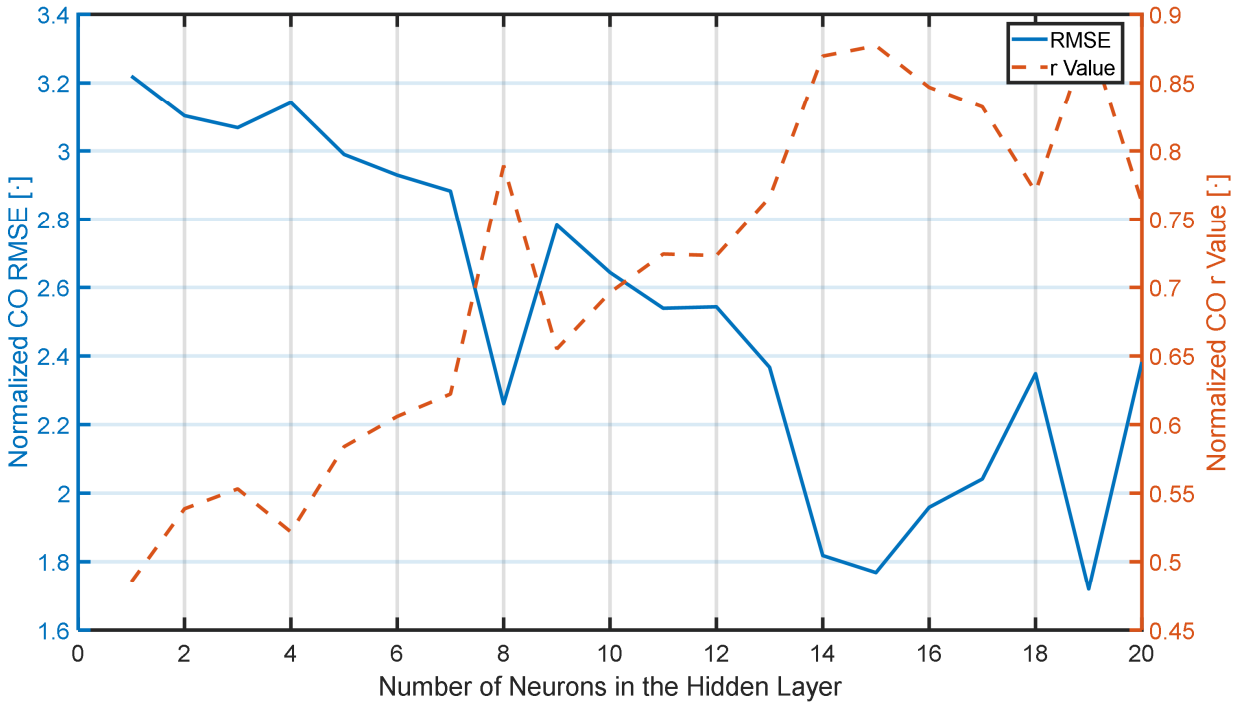

Figure 2. Dependence of the goodness of fit of the multi-layer perceptron (MLP) for cardiac output (CO) estimation (in terms of root-mean-squared error (RMSE) and correlation coefficient between measured vs. estimated CO) on the number of neurons in its hidden layer. Normalized RMSE and r value do not have units.

Table 1. Performance metrics associated with the CaRD algorithm and the BN algorithm. Explainability: The percentage of the 144 $\Delta I(t)$ values that are explainable ((i) $\Delta I(t) \geq 0$ when $\widetilde{Q} \leq 0$ or (i) $\Delta I(t) < 0$ when $\widetilde{Q} > 0$). Aggressiveness: The degree of change in the hourly IV fluid infusion rate, measured in terms of average $|\Delta I(t)|$ values. CO NAME: Normalized mean absolute error (NMAE) of 24, 12, and 9 h post-burn CO measurements with respect to the animal's pre-burn CO measurement in each animal. In-range CO rate: The number of post-burn CO measurements within the range of interest (given by $|\widetilde{Q}| \leq \widetilde{Q}_{threshold}$, where $\widetilde{Q}_{threshold}$ is the threshold specifying the in-range) divided by the total number of post-burn CO measurements.

		CaRD	**BN**
Explainability [%]		77.5	63.4
Aggressiveness [mL/h]		24.0	22.7
CO NMAE [-]	24 h	0.33 ± 0.12	0.33 ± 0.15
	12 h	0.32 ± 0.15	0.35 ± 0.24
	09 h	0.30 ± 0.18	0.34 ± 0.22
In-Range CO Rate [%]	$\lvert\widetilde{Q}\rvert \leq 1$	14.5 ± 14.9	17.7 ± 14.6
	$\lvert\widetilde{Q}\rvert \leq 2$	37.0 ± 20.0	35.0 ± 15.5

3.2. Algorithm Performance

The performance of the CaRD algorithm, both in terms of NMAE and in-range CO rate, was only marginally superior to that of the BN algorithm, although a statistical test was not performed due to the very small sample size (Figures 4 and 5, Table 1). Figures 4 and 5 show the performance of the CaRD algorithm in comparison with the BN algorithm in terms of (i) the normalized mean absolute error (NMAE) of 24, 12, and 9 h post-burn CO measurements with respect to the animal's pre-burn CO measurement and (ii) the in-range CO rate, respectively. Table 1 shows the numerical values of these metrics. First,

the CaRD algorithm showed a smaller average NMAE and its variability (in SD) than the BN algorithm (Figure 4). Second, the CaRD algorithm showed a larger in-range CO rate than the BN algorithm corresponding to $|\widetilde{Q}| \leq 2$ (Figure 5). However, considering the more stringent range of $|\widetilde{Q}| \leq 1$, neither of these algorithms appeared compelling. Figure 6 shows a representative example of (a) successful and (b) unsuccessful CaRD algorithm results, including UO and PPV, measured vs. estimated CO (with bounds indicating $|\widetilde{Q}| = 1$ and $|\widetilde{Q}| = 2$), IV fluid infusion rate, and the trajectory of the animal in the normalized UO-normalized PPV plane. The same results pertaining to all the animals associated with both the CaRD algorithm and the BN algorithm are visualized in the **Supplemental Materials**. In case of the CaRD algorithm, two animals were over-resuscitated (Animals 2–6 and 2–7 (in which 50% and 67% of CO measurements were above the $|\widetilde{Q}| \leq 2$ envelope, respectively; see **Supplemental Materials**)), one animal was under-resuscitated (Animal 2–10 (in which 89% of the CO measurements were below the $|\widetilde{Q}| \leq 2$ envelope; see **Supplemental Materials** and Figure 6b)), and two animals were adequately resuscitated (Animals 2–12 and 2–13 (in which 57% and 63% of the CO measurements were within the $|\widetilde{Q}| \leq 2$ envelope, respectively; see **Supplemental Materials** and Figure 6a)), all across the 24 h of resuscitation. In the case of the BN algorithm, three animals were over-resuscitated (Animals 2–4, 2–8, and 2–11 (in which 78%, 63%, and 50% of the CO measurements were above the $|\widetilde{Q}| \leq 2$ envelope, respectively; see **Supplemental Materials**)), no animal was under-resuscitated, and one animal was adequately resuscitated (Animal 2–2 (in which 75% of the CO measurements were within the $|\widetilde{Q}| \leq 2$ envelope; see **Supplemental Materials**)), all across the 24 h of resuscitation. In sum, most animals were over-/under-resuscitated in both algorithms.

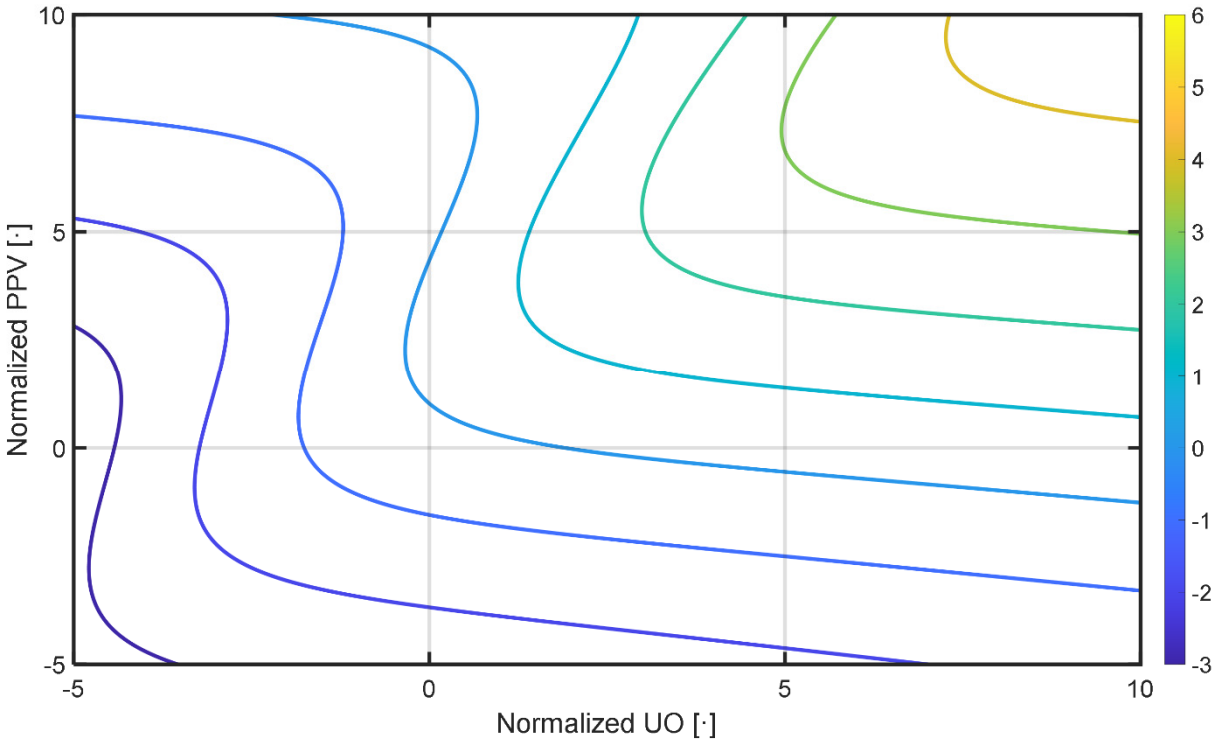

Figure 3. Regressed MLP mapping between normalized urinary output (UO), normalized pulse pressure variation (PPV), and normalized cardiac output (CO). Normalized PPV and normalized UO do not have units.

Table 2. Relationship between normalized UO ($\widetilde{U}$), normalized PPV ($\widetilde{\delta P_p}$), and normalized CO ($\widetilde{Q}$) in (a) development and (b) test datasets in terms of the number of input–output data pairs pertaining to each category. Colored cells indicate unexplainable input–output data pairs.

(a) $-1 \leq \widetilde{Q} \leq 1$			
	$\widetilde{\delta P_p} < -1$	$-1 \leq \widetilde{\delta P_p} \leq 1$	$\widetilde{\delta P_p} > 1$
$\widetilde{U} < -1$	2	2	6
$-1 \leq \widetilde{U} \leq 1$	1	1	4
$\widetilde{U} > 1$	9	0	4
(a) $\widetilde{Q} < -1$			
	$\widetilde{\delta P_p} < -1$	$-1 \leq \widetilde{\delta P_p} \leq 1$	$\widetilde{\delta P_p} > 1$
$\widetilde{U} < -1$	28	10	18
$-1 \leq \widetilde{U} \leq 1$	9	5	2
$\widetilde{U} > 1$	3	5	6
(a) $\widetilde{Q} > 1$			
	$\widetilde{\delta P_p} < -1$	$-1 \leq \widetilde{\delta P_p} \leq 1$	$\widetilde{\delta P_p} > 1$
$\widetilde{U} < -1$	0	1	4
$-1 \leq \widetilde{U} \leq 1$	1	1	0
$\widetilde{U} > 1$	2	2	18
(b) $-1 \leq \widetilde{Q} \leq 1$			
	$\widetilde{\delta P_p} < -1$	$-1 \leq \widetilde{\delta P_p} \leq 1$	$\widetilde{\delta P_p} > 1$
$\widetilde{U} < -1$	2	0	0
$-1 \leq \widetilde{U} \leq 1$	0	0	0
$\widetilde{U} > 1$	0	1	2
(b) $\widetilde{Q} < -1$			
	$\widetilde{\delta P_p} < -1$	$-1 \leq \widetilde{\delta P_p} \leq 1$	$\widetilde{\delta P_p} > 1$
$\widetilde{U} < -1$	0	2	1
$-1 \leq \widetilde{U} \leq 1$	0	2	1
$\widetilde{U} > 1$	1	6	5
(b) $\widetilde{Q} > 1$			
	$\widetilde{\delta P_p} < -1$	$-1 \leq \widetilde{\delta P_p} \leq 1$	$\widetilde{\delta P_p} > 1$
$\widetilde{U} < -1$	1	0	0
$-1 \leq \widetilde{U} \leq 1$	0	2	0
$\widetilde{U} > 1$	1	6	3

3.3. Algorithm Analysis

In our attempt to determine which aspect(s) in the CaRD algorithm must be improved to make it more efficacious, we conducted an extensive analysis to understand the behavior of the CaRD algorithm. We, in particular, analyzed individual elements in the CaRD algorithm, including (i) input normalization, (ii) CO estimation, and (iii) fluid dose recommendation.

First, the input normalization element may affect the CaRD algorithm performance through its sensitivity to inputs. To illustrate, the CaRD algorithm can perform more aggressive resuscitation if the spread parameters in Equations (1)–(3) are underestimated, while it can perform less aggressive resuscitation if the spread parameters are overestimated. To infer the appropriateness of the spread parameters used in the CaRD algorithm (i.e., those determined using the development dataset), we compared the spread parameters pertaining to PPV and CO determined from the development dataset vs. the test dataset. For PPV,

the spread parameters were 1.3% vs. 2.0%, respectively. For CO, the spread parameters were 9.0 mL/min/kg vs. 7.8 mL/min/kg, respectively. Hence, the spreads used in the CaRD algorithm appeared to be reasonable. Therefore, our analysis suggests that the spread parameters used in the CaRD algorithm may be used as is. Alternatively, they may be refined by leveraging both the development dataset and the test dataset.

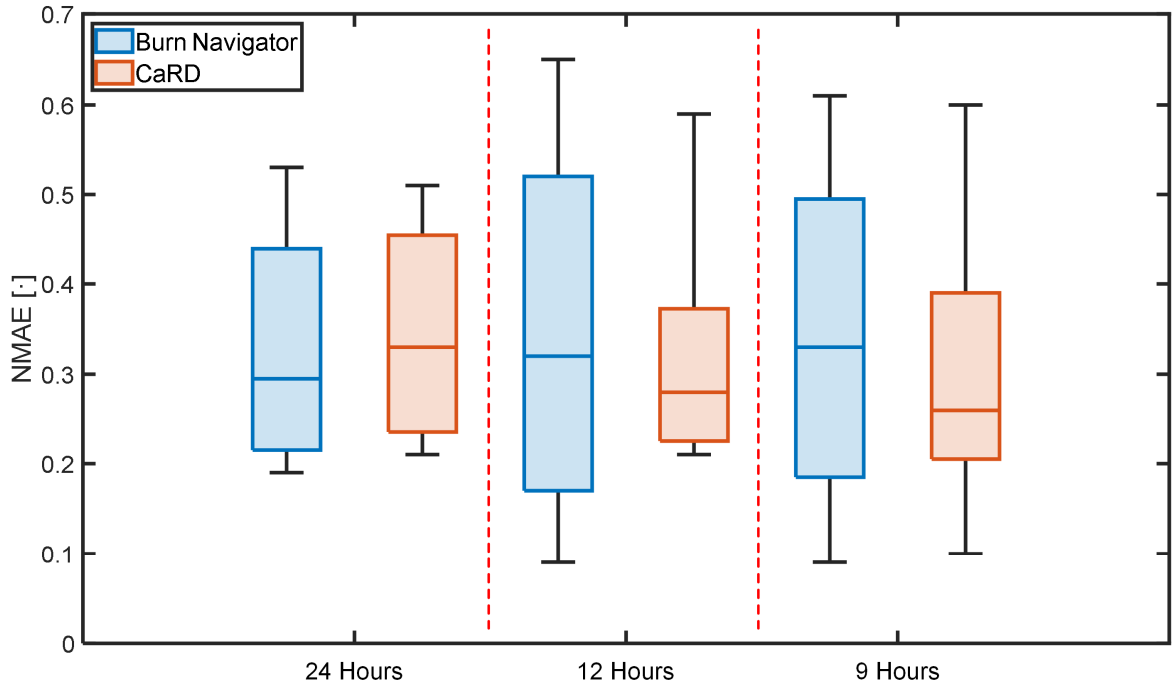

Figure 4. Normalized mean absolute error (NMAE) between 24, 12, and 9 h post-burn CO measurements and the animal's pre-burn CO measurement pertaining to both the CaRD algorithm and BN algorithm. NMAE does not have a unit.

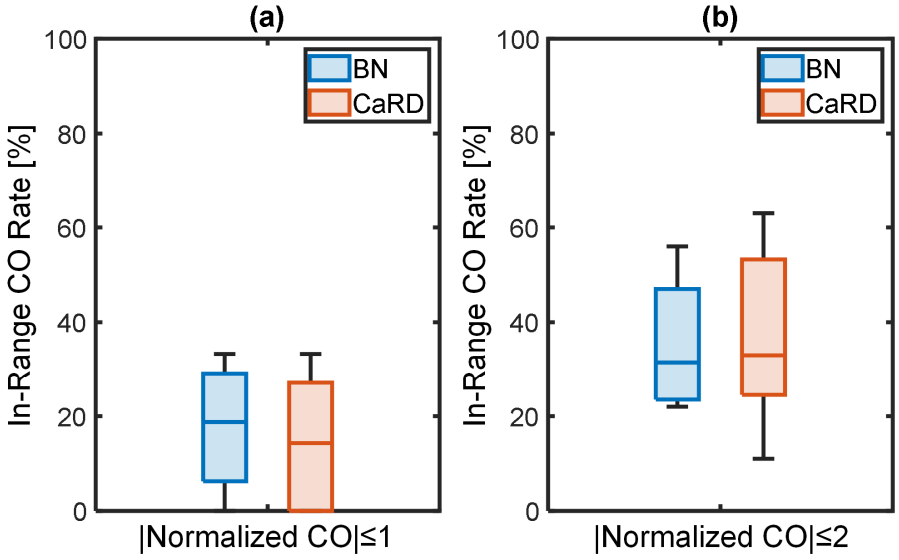

Figure 5. In-range CO rate pertaining to both the CaRD algorithm and BN algorithm, defined as the number of post-burn CO measurements within the range of interest (given by $|\widetilde{Q}| \leq \widetilde{Q}_{threshold}$, where $\widetilde{Q}_{threshold}$ is the threshold specifying the in-range) divided by the total number of post-burn CO measurements. (**a**) $\widetilde{Q}_{threshold} = 1$. (**b**) $\widetilde{Q}_{threshold} = 2$.

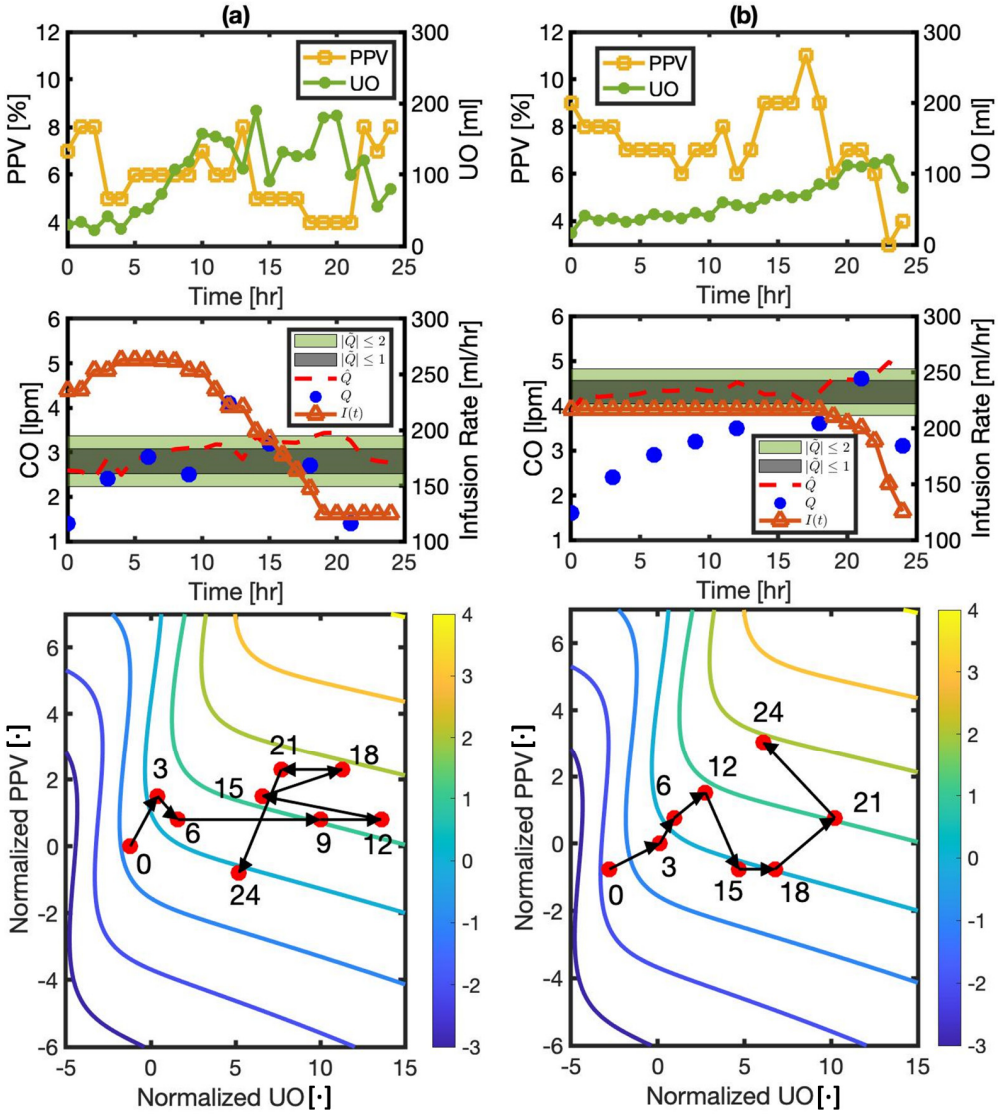

Figure 6. Representative example of (**a**) successful and (**b**) unsuccessful CaRD algorithm results, including UO and PPV, measured vs. estimated CO (with bounds indicating $|\tilde{Q}| = 1$ and $|\tilde{Q}| = 2$), IV fluid infusion rate, and the trajectory of the animal in the normalized UO-normalized PPV plane. $\hat{Q}$: estimated CO. Q: measured CO. Normalized PPV and normalized UP do not have units.

Second, the CO estimation element may affect the CaRD algorithm performance through its accuracy. Indeed, the performance of the CaRD algorithm may deteriorate if the CO estimation accuracy is poor. In particular, CaRD may over-resuscitate if CO is underestimated, while it may under-resuscitate if CO is overestimated. To understand the relationship between resuscitation adequacy vs. CO estimation error, we examined the correlation between them obtained from the test dataset. Figure 7 shows the correlation between CO estimation accuracy vs. CaRD resuscitation performance (in terms of NMAE between 24 h post-burn CO measurements vs. pre-burn CO measurement). As expected, they showed a proportional relationship (Figure 7). In addition, two animals associated with consistent CO underestimation (Animals 2–6 and 2–7) were drastically over-resuscitated (see Figure 6b for Animal 2–7), whereas one animal associated with consistent CO overestimation (Animal 2–10) was drastically under-resuscitated (see **Supplemental Materials**).

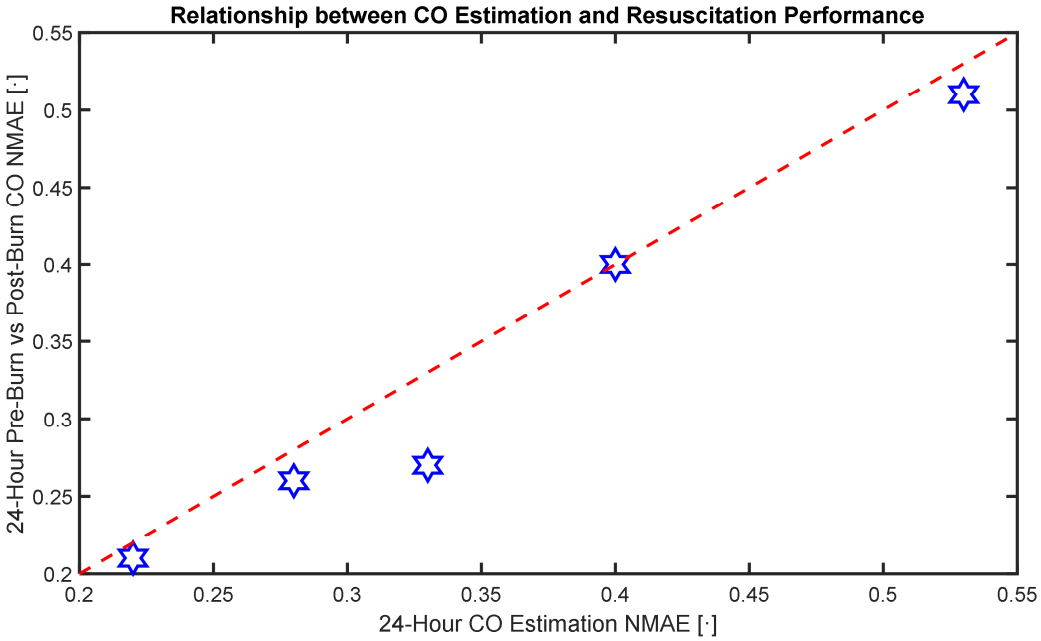

Figure 7. Correlation between CO estimation accuracy vs. CaRD resuscitation performance (in terms of NMAE between 24 h post-burn CO measurements vs. pre-burn CO measurement). NMAE does not have a unit.

Overall, CO estimation accuracy was not superb (35 ± 12% in terms of NMAE). We speculated that PPV and UO by themselves may not be sufficient to estimate CO accurately. To ascertain our conjecture, we (i) inspected the intuitive explainability of the relationship between normalized PPV, normalized UO, and normalized CO in both development and test datasets and (ii) examined the performance of the most powerful arterial PWA-based surrogate of CO found in our prior work relative to PPV. First, Table 2 summarizes the relationship between normalized PPV, normalized UO, and normalized CO in (a) development and (b) test datasets in terms of the number of input–output data pairs pertaining to each category. Inspecting normalized PPV, normalized UO, and normalized CO revealed that a nonnegligible subset of these measurement pairs was not intuitively explainable (see the red cells in Table 2). As an example, there were six input–output data pairs in which $\widetilde{U} > 1$ and $\delta\widetilde{P}_p > 1$ (indicating over-resuscitation) but $\widetilde{Q} < -1$ (indicating under-resuscitation; see Table 2a $\widetilde{Q} < -1$). As another example, there were six input–output data pairs in which $\widetilde{U} > 1$ and $-1 \leq \delta\widetilde{P}_p \leq 1$ (indicating moderate over-resuscitation) but $\widetilde{Q} < -1$ (indicating under-resuscitation; see Table 2b $\widetilde{Q} < -1$). All in all, only 81% of the input–output data pairs in the development dataset and 42% of the input–output data pairs in the test dataset were explainable (white cells in Table 2). These results suggest that PPV and UO may not provide sufficient information to allow for the accurate estimation of CO. Second, the combination of the most powerful arterial PWA-based surrogate of CO from our prior work (i.e., $\frac{P_m - P_d}{T}$) and UO modestly outperformed the PPV–UO pair: MAE decreased from 1.1 ± 0.6 lpm to 0.9 ± 0.4 lpm and, likewise, NMAE decreased from 35 ± 12% to 30 ± 12%. Regardless, the accuracy was still not superb in the absolute sense. Combined, our analysis suggests that novel biomarker(s) of CO, superior to arterial PWA-based surrogates and relevant to burn resuscitation settings, may need to be developed.

Third, similarly to its input normalization counterpart, the fluid dose recommendation element may affect the CaRD algorithm performance through its sensitivity to inputs (namely, PPV and UO), i.e., resuscitation aggressiveness. Indeed, if the "gain" of the fluid dose recommendation element is large, the CaRD algorithm may recommend more drastic fluid dose changes for a given change in CO estimate, which may benefit the resuscitation

performance but, at the same time, may increase the risk of over-/under-resuscitation. In contrast, if the gain of the fluid dose recommendation element is small, the CaRD algorithm may recommend more moderate fluid dose changes for a given change in CO estimate, which may negatively affect the resuscitation performance but, at the same time, may decrease the risk of over-/under-resuscitation. Figure 8 compares the distributions of (a) normalized CO in the CaRD algorithm vs. normalized UO in the BN algorithm and (b) the change in hourly IV fluid infusion rates pertaining to the CaRD algorithm vs. the BN algorithm, associated with both the development dataset and test dataset. Relative to the BN algorithm, the CaRD algorithm appeared to be more aggressive: the input to the CaRD algorithm (namely, normalized CO estimate) was more concentrated than the input to the BN algorithm (namely, normalized UO) (Figure 8a), while the range of hour-by-hour fluid dose change recommendation pertaining to the CaRD algorithm was much wider than the range pertaining to the BN algorithm with many extremely large values (Figure 8b). Despite its aggressiveness, however, the majority of the recommendations (80.4%) did not hit the ±20% (Animals 2–6, 2–7, 2–10) or ±10% (Animals 2–12 and 2–13) bounds, meaning that the gain of the CaRD algorithm is not unacceptably large. Regardless, the extremely large fluid dose changes recommended by the CaRD algorithm were mostly associated with the rapid increase in the fluid dose resulting in over-resuscitation (e.g., Animals 2–6 and 2–7; see **Supplemental Materials**). Therefore, our analysis suggests that the CaRD algorithm may need to be modestly desensitized, e.g., by adopting a smaller value of α in Equation (5).

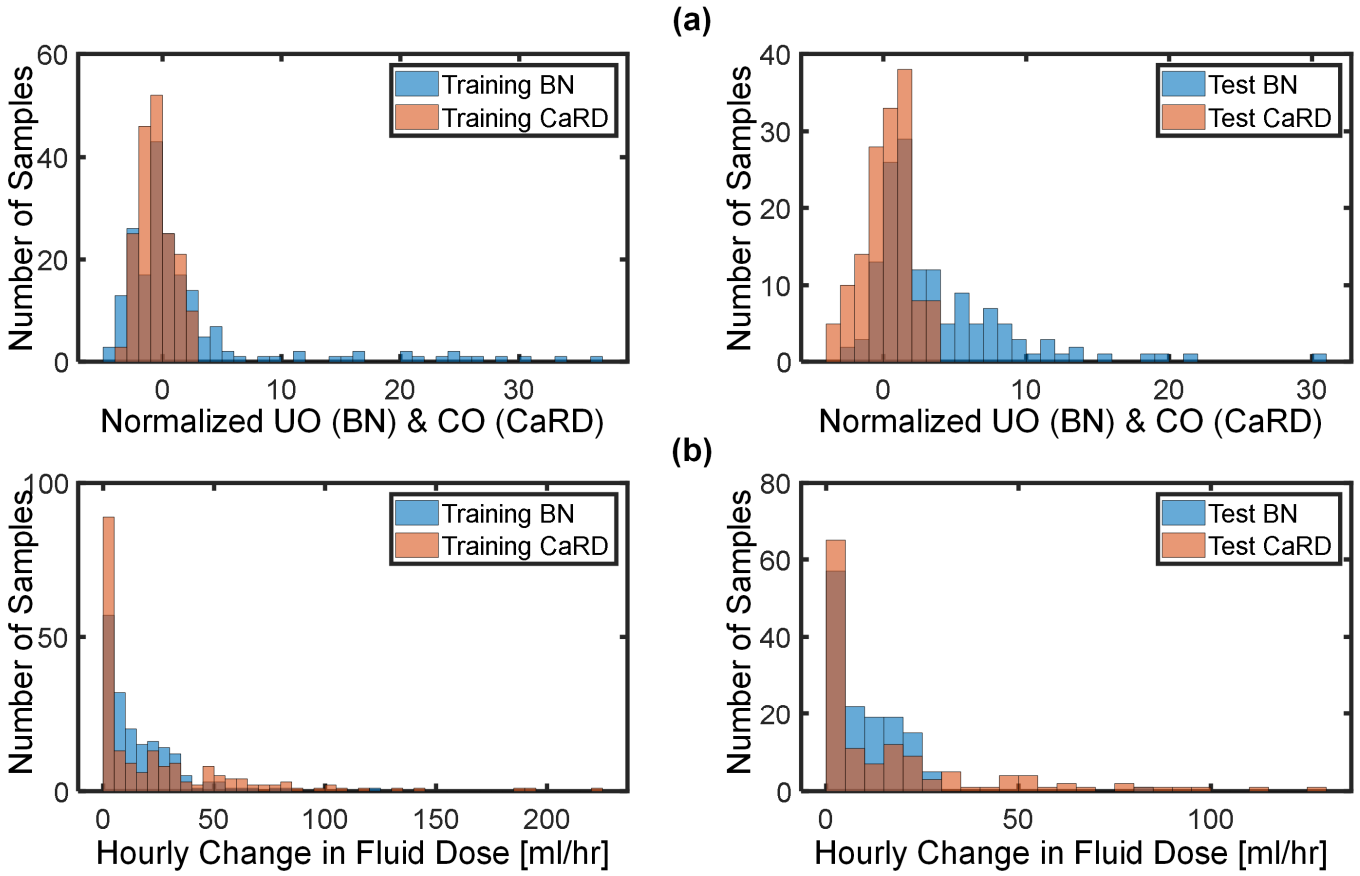

Figure 8. Distributions of (**a**) normalized CO in the CaRD algorithm vs. normalized UO in the BN algorithm and (**b**) the change in hourly IV fluid infusion rates pertaining to the CaRD algorithm vs. the BN algorithm associated with the development dataset (left panel) and test dataset (right panel).

4. Conclusions

Our initial effort to develop a context-aware burn resuscitation decision-support algorithm, the CaRD algorithm, showed both promise and limitations to overcome. Our work represents a pioneering investigation to improve burn resuscitation by incorporating context-aware surrogates of CO, which has not been explored in the existing body of literature to the best of our knowledge. In this regard, our work may stimulate the development of more advanced burn resuscitation decision-support algorithms guided by superior CO surrogates. However, at the same time, our initial evaluation and analysis of the CaRD algorithm revealed that future efforts must be exerted to improve the performance and safety of the CaRD algorithm. Specific possibilities include (i) developing more accurate CO estimation algorithms based on, e.g., additional context-aware surrogates and/or advanced machine learning algorithms, as well as (ii) optimizing the aggressiveness of the fluid dose recommendation algorithm based on follow-up experiments and data analysis. These improvements may necessitate additional physiological measurements and/or computationally expensive algorithms. Regardless, once these requisite enhancements can be achieved, the CaRD algorithm may enable superior burn care through (i) precise assessment of tissue perfusion state in a burn patient and (ii) optimal administration of resuscitation fluids to normalize the tissue perfusion in the patient. In addition, to realize true deployment at the bedside, this algorithm will need to be integrated with real-time automated physiological signal processing algorithms and analytics.

Supplementary Materials: The following supporting information can be downloaded at https://www.mdpi.com/article/10.3390/electronics13142713/s1, UO and PPV, measured vs. estimated CO (with bounds indicating $|\widetilde{Q}| = 1$ and $|\widetilde{Q}| = 2$), IV fluid infusion rate, and the trajectory in the normalized UO-normalized PPV plane pertaining to all the animals associated with both the CaRD algorithm and the BN algorithm.

Author Contributions: Conceptualization, J.-O.H. and D.M.B.; methodology, J.-O.H. and D.M.B.; software, Y.-M.K. and G.A.; validation, Y.-M.K. and J.-O.H.; formal analysis, Y.-M.K. and J.-O.H.; investigation, Y.-M.K., B.P., D.M.B. and J.-O.H.; resources, J.-O.H. and D.M.B.; data curation, D.M.B., B.P., E.E.Z., M.M.M., C.S.D., M.O., L.M., S.K.M., E.J.K., B.C.C. and J.W.S.; writing—original draft preparation, Y.-M.K. and J.-O.H.; writing—review and editing, G.A., B.P., D.M.B., E.E.Z., M.M.M., C.S.D., M.O., L.M., S.K.M., E.J.K., B.C.C. and J.W.S.; supervision, J.-O.H. and D.M.B.; project administration, J.-O.H. and D.M.B. All authors have read and agreed to the published version of the manuscript.

Funding: This work was supported in part by CDMRP under Grants W81XWH-19-2-0004 and W81XWH-19-1-0322.

Institutional Review Board Statement: This research was approved by the MedStar Health Research Institutional Animal Care and Use Committee (IACUC) and performed at an AAALAC fully accredited facility with protocol numbers 2003001092 (2020-005) and 2304010131 (2023-009). All animal procedures were conducted in compliance with the Guide for the Care and Use of Laboratory Animals and the Animal Welfare Act.

Data Availability Statement: The raw data supporting the conclusions of this article will be made available by the authors on request.

Conflicts of Interest: The authors declare no conflicts of interest.

References

1. Jeschke, M.G.; van Baar, M.E.; Choudhry, M.A.; Chung, K.K.; Gibran, N.S.; Logsetty, S. Burn Injury. *Nat. Rev. Dis. Prim.* **2020**, *6*, 11. [CrossRef] [PubMed]
2. Nielson, C.B.; Duethman, N.C.; Howard, J.M.; Moncure, M.; Wood, J.G. Burns: Pathophysiology of Systemic Complications and Current Management. *J. Burn Care Res.* **2017**, *38*, e469–e481. [CrossRef] [PubMed]
3. Wurzer, P.; Culnan, D.; Cancio, L.C.; Kramer, G.C. Pathophysiology of Burn Shock and Burn Edema. In *Total Burn Care*, 5th ed.; Elsevier: Amsterdam, The Netherlands, 2017; pp. 66–76.e3, ISBN 9780323476614.
4. Greenhalgh, D.G. Burn Resuscitation: The Results of the ISBI/ABA Survey. *Burns* **2010**, *36*, 176–182. [CrossRef] [PubMed]

5. Cancio, L.C.; Bohanon, F.J.; Kramer, G.C. Burn Resuscitation. In *Total Burn Care*, 5th ed.; Elsevier: Amsterdam, The Netherlands, 2017; pp. 77–86.e2.
6. Rae, L.; Fidler, P.; Gibran, N. The Physiologic Basis of Burn Shock and the Need for Aggressive Fluid Resuscitation. *Crit. Care Clin.* **2016**, *32*, 491–505. [CrossRef] [PubMed]
7. Caruso, D.M.; Matthews, M.R. Monitoring End Points of Burn Resuscitation. *Crit. Care Clin.* **2016**, *32*, 525–537. [CrossRef] [PubMed]
8. Burmeister, D.M.; Smith, S.L.; Muthumalaiappan, K.; Hill, D.M.; Moffatt, L.T.; Carlson, D.L.; Kubasiak, J.C.; Chung, K.K.; Wade, C.E.; Cancio, L.C.; et al. An Assessment of Research Priorities to Dampen the Pendulum Swing of Burn Resuscitation. *J. Burn Care Res.* **2021**, *42*, 113–125. [CrossRef] [PubMed]
9. Cancio, L.C.; Salinas, J.; Kramer, G.C. Protocolized Resuscitation of Burn Patients. *Crit. Care Clin.* **2016**, *32*, 599–610. [CrossRef] [PubMed]
10. Paratz, J.D.; Stockton, K.; Paratz, E.D.; Blot, S.; Muller, M.; Lipman, J.; Boots, R.J. Burn Resuscitation-Hourly Urine Output versus Alternative Endpoints: A Systematic Review. *Shock* **2014**, *42*, 295–306. [CrossRef]
11. Cartotto, R.; Greenhalgh, D.G.; Cancio, C. Burn State of the Science: Fluid Resuscitation. *J. Burn Care Res.* **2017**, *38*, e596–e604. [CrossRef]
12. Davenport, L.M.; Dobson, G.P.; Letson, H.L. The Role of Invasive Monitoring in the Resuscitation of Major Burns: A Systematic Review and Meta-Analysis. *Int. J. Burns Trauma* **2019**, *9*, 28.
13. Dries, D.J.; Waxman, K. Adequate Resuscitation of Burn Patients May Not Be Measured by Urine Output and Vital Signs. *Crit. Care Med.* **1991**, *19*, 327–329. [CrossRef] [PubMed]
14. Peeters, Y.; Lebeer, M.; Wise, R.; Malbrain, M.L.N.G. An Overview on Fluid Resuscitation and Resuscitation Endpoints in Burns: Past, Present and Future. Part 2—Avoiding Complications by Using the Right Endpoints with a New Personalized Protocolized Approach. *Anaesthesiol. Intensive Ther.* **2015**, *47*, s15–s26. [CrossRef]
15. Latenser, B.A. Critical Care of the Burn Patient: The First 48 Hours. *Crit. Care Med.* **2009**, *37*, 2819–2826. [CrossRef] [PubMed]
16. Berkenstadt, H.; Friedman, Z.; Preisman, S.; Keidan, I.; Livingstone, D.; Perel, A. Pulse Pressure and Stroke Volume Variations during Severe Haemorrhage in Ventilated Dogs. *Br. J. Anaesth.* **2005**, *94*, 721–726. [CrossRef] [PubMed]
17. Westphal, G.; Garrido, A.D.P.G.; De Almeida, D.P.; Rocha E Silva, M.; Poli-De-Figueiredo, L.F. Pulse Pressure Respiratory Variation as an Early Marker of Cardiac Output Fall in Experimental Hemorrhagic Shock. *Artif. Organs* **2007**, *31*, 284–289. [CrossRef] [PubMed]
18. Sano, H.; Seo, J.; Wightman, P.; Cave, N.J.; Gieseg, M.A.; Johnson, C.B.; Chambers, P. Evaluation of Pulse Pressure Variation and Pleth Variability Index to Predict Fluid Responsiveness in Mechanically Ventilated Isoflurane-Anesthetized Dogs. *J. Vet. Emerg. Crit. Care* **2018**, *28*, 301–309. [CrossRef] [PubMed]
19. Johnson, M.C.; Alarhayem, A.; Convertino, V.; Carter, R.; Chung, K.; Stewart, R.; Myers, J.; Dent, D.; Liao, L.; Cestero, R.; et al. Compensatory Reserve Index: Performance of a Novel Monitoring Technology to Identify the Bleeding Trauma Patient. *Shock* **2018**, *49*, 295–300. [CrossRef] [PubMed]
20. Johnson, M.C.; Alarhayem, A.; Convertino, V.; Carter, R.; Chung, K.; Stewart, R.; Myers, J.; Dent, D.; Liao, L.; Cestero, R.; et al. Comparison of Compensatory Reserve and Arterial Lactate as Markers of Shock and Resuscitation. *J. Trauma Acute Care Surg.* **2017**, *83*, 603–608. [CrossRef] [PubMed]
21. Stewart, C.L.; Mulligan, J.; Grudic, G.Z.; Pyle, L.; Moulton, S.L. A Noninvasive Computational Method for Fluid Resuscitation Monitoring in Pediatric Burns: A Preliminary Report. *J. Burn Care Res.* **2015**, *36*, 145–150. [CrossRef]
22. Kimball, J.P.; Zia, J.S.; An, S.; Rolfes, C.; Hahn, J.O.; Sawka, M.N.; Inan, O.T. Unifying the Estimation of Blood Volume Decompensation Status in a Porcine Model of Relative and Absolute Hypovolemia Via Wearable Sensing. *IEEE J. Biomed. Health Inf.* **2021**, *25*, 3351–3360. [CrossRef]
23. Zia, J.; Kimball, J.; Rolfes, C.; Hahn, J.-O.; Inan, O.T. Enabling the Assessment of Trauma-Induced Hemorrhage via Smart Wearable Systems. *Sci. Adv.* **2020**, *6*, eabb1708. [CrossRef]
24. Wasicek, P.J.; Teeter, W.A.; Yang, S.; Hu, P.; Gamble, W.B.; Galvagno, S.M.; Hoehn, M.R.; Scalea, T.M.; Morrison, J.J. Arterial Waveform Morphomics during Hemorrhagic Shock. *Eur. J. Trauma Emerg. Surg.* **2021**, *47*, 325–332. [CrossRef]
25. Pottecher, J.; Chemla, D.; Xavier, L.; Liu, N.; Chazot, T.; Marescaux, J.; Fischler, M.; Diemunsch, P.; Duranteau, J. The Pulse Pressure/Heart Rate Ratio as a Marker of Stroke Volume Changes during Hemorrhagic Shock and Resuscitation in Anesthetized Swine. *J. Trauma Acute Care Surg.* **2013**, *74*, 1438–1445. [CrossRef]
26. Sirio, C.A. Critical Care Performance Measurement: The Time Has Come for All. *Crit. Care Med.* **2006**, *34*, 1538–1539. [CrossRef]
27. Dark, P.; Little, R.; Nirmalan, M.; Purdy, J. Systemic Arterial Pressure Wave Reflections during Acute Hemorrhage. *Crit. Care Med.* **2006**, *34*, 1497–1505. [CrossRef]
28. Arabidarrehdor, G.; Kao, Y.M.; Oliver, M.A.; Parajuli, B.; Carney, B.C.; Keyloun, J.W.; Moffatt, L.T.; Shupp, J.W.; Hahn, J.O.; Burmeister, D.M. The Potential of Arterial Pulse Wave Analysis in Burn Resuscitation: A Pilot In Vivo Study. *J. Burn Care Res.* **2023**, *44*, 599–609. [CrossRef]
29. Pham, T.N.; Cancio Leopoldo, C.; Gibran, N.S. American Burn Association Practice Guidelines Burn Shock Resuscitation. *J. Burn Care Res.* **2008**, *29*, 257–266. [CrossRef]
30. Endorf, F.W.; Dries, D.J. Burn Resuscitation. *Scand. J. Trauma Resusc. Emerg. Med.* **2011**, *19*, 69. [CrossRef]
31. Salinas, J.; Kramer, G.C.; Drew, G.A. Burn Patient Resuscitation System. U.S. Patent US8597273B2, 3 December 2013.

32. Salinas, J.; Chung, K.K.; Mann, E.A.; Cancio, L.C.; Kramer, G.C.; Serio-Melvin, M.L.; Renz, E.M.; Wade, C.E.; Wolf, S.E. Computerized Decision Support System Improves Fluid Resuscitation following Severe Burns: An Original Study. *Crit. Care Med.* **2011**, *39*, 2031–2038. [CrossRef]
33. Cartotto, R.; Burmeister, D.M.; Kubasiak, J.C. Burn Shock and Resuscitation: Review and State of the Science. *J. Burn Care Res.* **2022**, *43*, 567–585. [CrossRef]
34. Dhondt, L.; Croubels, S.; De Paepe, P.; Wallis, S.C.; Pandey, S.; Roberts, J.A.; Lipman, J.; De Cock, P.; Devreese, M. Conventional Pig as Animal Model for Human Renal Drug Excretion Processes: Unravelling the Porcine Renal Function by Use of a Cocktail of Exogenous Markers. *Front. Pharmacol.* **2020**, *11*, 883. [CrossRef]
35. Burmeister, D.M.; Supp, D.M.; Clark, R.A.; Tredget, E.E.; Powell, H.M.; Enkhbaatar, P.; Bohannon, J.K.; Cancio, L.C.; Hill, D.M.; Nygaard, R.M. Advantages and Disadvantages of Using Small and Large Animals in Burn Research: Proceedings of the 2021 Research Special Interest Group. *J. Burn Care Res.* **2022**, *43*, 1032–1041. [CrossRef]
36. Michard, F.; Boussat, S.; Chemla, D.; Anguel, N.; Mercat, A.; Lecarpentier, Y.; Richard, C.; Pinsky, M.R.; Teboul, J.-L. Relation between Respiratory Changes in Arterial Pulse Pressure and Fluid Responsiveness in Septic Patients with Acute Circulatory Failure. *Am. J. Respir. Crit. Care Med.* **2000**, *162*, 134–138. [CrossRef] [PubMed]

Disclaimer/Publisher's Note: The statements, opinions and data contained in all publications are solely those of the individual author(s) and contributor(s) and not of MDPI and/or the editor(s). MDPI and/or the editor(s) disclaim responsibility for any injury to people or property resulting from any ideas, methods, instructions or products referred to in the content.